Available online at www.sciencedirect.com
SCIENCE DIRECT®
Journal of Nuclear Materials 341 (2005) 31–44
journal of nuclear materials
www.elsevier.com/locate/jnucmat

Oxidative erosion of graphite in air between 600 and 1000 K

M. Balden *, K.U. Klages, W. Jacob, J. Roth

Max-Planck-Institut für Plasmaphysik, EURATOM Association, Boltzmannstr. 2, D-85748 Garching, Germany

Received 30 June 2004; accepted 7 January 2005

Abstract

The oxidative erosion of seven types of graphite has been investigated by heating in air at temperatures between 600 and 1000 K. The specimens include pyrolytic graphite, fine-grain graphites, carbon-fibre composites (CFC), and graphites doped with Si and Ti. The weight loss was measured using a microbalance, the surface morphology by scanning electron microscopy, and the composition of the surface layer by MeV ion beam techniques. Pyrolytic graphite is least affected by erosion, while pure and Si-doped CFCs erode particularly fast. Typical erosion rates for specimens with a surface area of $\simeq$4 cm^2 are below 0.2 μg/m^2 s at 600 K for all graphite types, and at 900 K range from 0.34 mg/m^2 s for pyrolytic graphite to about 9 mg/m^2 s for the strongest eroding types. The temperature dependence of the erosion rate of all types of graphite studied is well described by an activation energy of 1.7 eV. The erosion rates of these graphites are by far lower than the removal rates for deposited amorphous hydrocarbon layers. In contrast to all other types, the Ti-doped graphite absorbs a significant amount of oxygen reaching up to $\simeq$5% of its original mass. Once the oxygen uptake is saturated, it erodes with rates similar to those of the strongest eroding types.

1. Introduction

Carbon materials are widely used in today's fusion plasma experiments and their utilisation is planned in future thermonuclear fusion reactors [1–3]. Unfortunately, carbon has a high chemical reactivity with hydrogen atoms and ions [4,5]. This causes erosion yields of the order of several 10^{-2} for deuterium ion energies ranging from several keV down to a few eV. These high erosion yields lead to plasma dilution, limited component lifetime, and a large tritium inventory in re-deposited carbon layers. Therefore, the most recent ITER design [2,6] attempts to limit the use of carbon as much as possible, restricting it to surface areas of extreme heat load.

A low tritium inventory is important for safety considerations. Much effort has been spent in the last years to develop strategies and methods to remove the tritium from re-deposited carbon layers (for a review see [1]). Some of the suggested methods operate with oxygen in the vessel at elevated temperature. Therefore, the erosion behaviour of amorphous hydrogenated carbon (a-C:H) layers due to heating in air or oxygen and the thermal desorption were investigated in detail by several groups [1,7–19]. The temperatures suggested for removal by heating in oxygen are below 700 K [11,12].

For all removal techniques, especially those operating with oxygen, the effects on the carbon base materials have to be determined [20–22]. Recently, the database for oxidative erosion rates of carbon materials has been reviewed [23]. It was concluded that co-deposited layers can be effectively removed without significant erosion of the carbon base materials.

* Corresponding author. Tel.: +49 89 3299 1688; fax: +49 89 3299 1212.
E-mail address: martin.balden@ipp.mpg.de (M. Balden).

0022-3115/$ - see front matter © 2005 Elsevier B.V. All rights reserved.
doi:10.1016/j.jnucmat.2005.01.006

Furthermore, examining the oxidation of the carbon base materials is an important task in accident analyses for fusion reactors, e.g., air ingress into the vacuum vessel (LOVA = loss of vacuum accident) or rupture of a water-cooling tube connected to the vacuum (LOCIV = loss of coolant into vacuum) [6,24,25]. The reaction products with O_2 are CO and CO_2, and with H_2O additionally H_2. Both accident scenarios may produce combustible gases (H_2, CO) and release radioactive material (tritium, activated dust). Investigations on such accident analyses [20,26–30] were carried out above 900 K, where the in-pore diffusion of the gases is the rate limiting process. At higher temperatures (>1200 K), the mass transfer to and away from the surface is the slowest step and, as a result, the erosion is only slightly temperature dependent [21,28,31,32]. For lower temperatures (<900 K) the chemical reaction between oxygen and carbon is the rate limiting process [27,28,33,34]. The transition temperatures between the different ranges depent on various parameters such as specimen porosity, microscopic structure, specimen shape and size, partial and total pressure, and the presence of water vapour [26,28]. The kinetic energy of molecular oxygen also affects the oxidation behaviour [14,31,32].

For Si-doped graphites, silicon does not reduce the oxidative erosion rates by heating in air up to 1000 K [26,35]. At higher temperatures the presence of Si improves the oxidation resistance of carbon fibre-reinforced composite materials (CFCs), especially the reaction with steam [26,36]. It has been suggested that a protective SiO_2 layer forms on the surface of the material under these conditions [30,36].

In this paper, we report on the oxidative erosion behaviour of a variety of carbon materials by heating in air for temperatures ranging from 600 to 1000 K and for heating durations between 1 and 80 h [22]. The erosion was observed by weight loss and by changes of the surface morphology for specimens of seven different materials: pyrolytic graphite, fine-grain graphites, CFCs, and doped carbon materials. The intention of doping the graphite is to prevent the chemical erosion due to interaction with hydrogen, i.e., to increase the lifetime compared to pure graphite components in hydrogen environment [37,38]. The oxygen uptake, especially for the doped materials, was measured in order to investigate the formation of oxides.

2. Experimental

2.1. Materials and specimens

Some properties of the graphites selected and the names of the specimen types, which are used throughout the paper, are summarised in Table 1.

All seven materials were previously employed for studies on the chemical erosion behaviour of carbon by hydrogen impact [39–42]. The CFC material NB31

Table 1
Properties of investigated graphites

Name	Description	Density (g/cm^3)	Composition	Manufacturer	Figures
HPG⊥ HPG‖	Pyrolytic graphite, grade HPG, cut perpendicular (HPG⊥) and parallel (HPG‖) to the preferred orientation of the graphitic planes, mosaic spread of ≃30°	2.24 (99% ρ_{th})	Pure C	Union Carbide, USA	1,2,5 1,2,4
AXF-5Q	Fine grain graphite mainly open pores	1.85 (82% ρ_{th})	Pure C	Poco Inc., USA	1,2,6
EK98	Fine grain graphite mainly closed pores	1.86 (82% ρ_{th})	Pure C	SGL Carbon AG, Germany	1,2,7
N112	3-dimensional carbon fibre composite (CFC) of ex-PAN fibres; densified by chemical vapour infiltration, graphitised, and finally impregnated with pitch	1.95 (86% ρ_{th})	Pure C	SEPCARB, SNECMA, France	1,2,8
NB31	CFC; 3-dimensional fibre architecture partly of ex-pitch fibres; densification, graphitization, and impregnation like N112	1.90 (84% ρ_{th})	Pure C	SEPCARB, SNECMA, France	1,2,9
NS31	CFC like NB31, but impregnation in liquid Si instead of pitch	2.0	C + 8–10 at.% Si	SEPCARB, SNECMA, France	1–3,10,12
RGi91	Anisotropic fine-grain graphite doped with Ti (uniaxial pressed powder mixture of Ti and graphite, heated at high temperature)	–	C + 2 at.% Ti	Ischranov Institute Moscow, Russia	1–3,11,13

All materials were delivered before 1998. The theoretical density of graphite is ρ_{th} = 2.26 g/cm^3.

is the reference carbon material for ITER [6,43,44] and NS31 is a possible doped candidate [6,44].

The specimens were cut with a diamond saw from large blocks to small plates of approximately $15 \times 12 \times 1\ mm^3$. They were then cleaned in an ultrasonic bath. No further surface preparation was carried out.

The original masses of the specimens were usually between 0.3 and 0.4 g. To avoid weight loss due to gas release during heating in air, the specimens were annealed in vacuum for 2 h at ≃1020 K prior to the erosion experiments. The mass of the different specimens of one type varied by less than 10% for HPG⊥ and HPG‖, approximately 30% for AXF-5Q and NS31, and around 20% for the other four graphites. The macroscopic surface area of the specimens was always close to $4\ cm^2$. It should be noted that the microscopic area is not known while the macroscopic area of the specimens is well known. The microscopic area is attacked by the oxidative erosion and is correlated to the porosity. For NB31 and NS31 the reported specific surface area – measured by a gas-adsorption method developed by Brunauer, Emmett, and Teller (BET [45]) – is about 330 times larger than the macroscopic area [26].

The pyrolytic graphite HPG has a preferred orientation of the graphitic planes with a mosaic spread of ≃30°. The two first specimen types (Table 1) were cut from the same block of HPG, so that the larger surfaces of the plates were mainly oriented perpendicular (⊥) and parallel (‖) to the graphitic planes, respectively.

2.2. Oxidative erosion

The specimens were heated in air at temperatures between 600 and 1000 K for various durations (up to 80 h). The main analysis for the oxidative erosion consisted in weighing each specimen before and after each heating step. Specimens of all eight types of graphite (Table 1), i.e., a set of specimens, were simultaneously heated to ensure the same experimental conditions.

The measurements were performed in three types of series: a 'screening series', several 'temperature series', and three 'time series'. In the 'screening series', one set of specimens was heated at 600 K for 1 h and then further heated sequentially up to 1000 K in 100 K steps with 1 h dwell time. In the 'temperature series', sets of specimens were heated at fixed temperatures between 600 and 1000 K for 1 h. For each temperature a new set of specimens was used. In the three 'time series', three sets of specimens were heated at 600, 800, and 900 K for longer durations of up to 80 h. The heating was interrupted by weight measurements to obtain the time dependence of the mass change. For RGTi91, additional specimens were heated to study the oxygen uptake.

The temperature inside the furnace was monitored using a thermocouple. The temperature generally oscillated with an amplitude of ±15 K in cycles of 10–15 min. For heating at the temperature limit of the furnace (1000 K) and during the 'time series' at 800 K the oscillation amplitude increased to ±30 K. The specimens were always introduced into the furnace at a maximum of the temperature oscillation. The cooling of the specimen to room temperature (temperature of the balance) took approximately 5 min. The time needed to reach the desired temperature inside the furnace was estimated to be less than 5 min.

The furnace did not have an active control of the gas phase, i.e., the oxygen flow and humidity were not controlled. Air was only exchanged by opening the furnace for the weight measurements and by natural convection inside the furnace, which had a volume of ≃80 l.

A microbalance (Sartorius Ultramicro) was used for all weight measurements except for the 'time series' at 600 K, which was measured with another microbalance (Sartorius MC21S). To obtain an accuracy of 1 and 2 μg for the respective balance, at least three single measurements were performed. In order to evaluate the effects of specimen handling, an N112 specimen was lifted and put down 50 times with a pair of tweezers. The resulting mass change was −3 μg, i.e., a mass loss of 3 μg. Therefore, the systematic error due to normal handling is smaller than the accuracy of the weight measurement. For comparison, the mass loss by heating N112 for 1 h at 800 K is 244 μg, whereas for 80 h at 600 K it is only 20 μg.

2.3. Composition and surface morphology

The composition of the specimens was analysed by ion beam analysis using 2.5 MeV protons and 4 MeV ^4He ions at a scattering angle of 165° [46]. The program SIMNRA [47] was used to determine the amount of oxygen with a detection limit of 0.3 and 1 at.% O up to about 3 and 1 μm for proton and He scattering, respectively. The Ti and Si content in the RGTi91 and NS31 specimens were also determined by ion beam analysis.

To investigate changes of the surface morphology of the specimens due to heating in air, scanning electron microscopy (SEM) was performed on specimens of each type of graphite before and after heating [48]. A mixture of secondary and back scattered electrons generated by a 20 keV electron beam were used for the imaging. The elemental composition was checked by energy dispersive X-ray spectroscopy (EDX) using a 10 keV electron beam [48].

3. Results and discussion

The results for the Ti-doped graphite, RGTi91, are discussed in a separate section because of its special behaviour. Despite that, the data are already presented for completeness in the figures of the following sections.

3.1. Mass changes and erosion rates

Throughout this section, the erosion of the specimens is characterised by their change in mass. In principle, if the erosion takes place only on the surface, the mass change (i.e., carbon erosion) must be correlated with the microscopic surface area of the specimens and not with their total mass. The microscopic surface area – a specific property of the material – is not known and could vary with the type of graphite. Nevertheless, the macroscopic surface area of all specimens is nearly the same (4 cm^2) and it is assumed that the slightly different initial masses of specimens of the same type of graphite are due to the difference in their thickness. Therefore, a surface area of 4 cm^2 is used to determine all erosion rates.

3.1.1. 'Time series': time dependence at constant temperature

Fig. 1 shows the time dependence of the mass loss of the different specimen types during isothermal heating at 600, 800, and 900 K. Note that the mass scales differ by four orders of magnitude between Figs. 1(a) and (c). In the following, the evaluation of the erosion rates is separately described for each temperature.

For heating at 600 K, the mass changes are very low: After 80 h at 600 K they are all lower than 25 μg (NS31). After heating for 15 h, the erosion for all types of specimen becomes about linear with time which means constant erosion rate. These rates scaled to kg/m^2 s are presented versus the reciprocal temperature in Fig. 2. N112, NB31, and NS31 show a different behaviour from the other four: They have a higher erosion rate at short heating times (below 15 h), i.e., at low burn-off. Such a behaviour was previously observed on pyrolytic graphite [49,50] and was interpreted as the erosion of areas where the graphitic order is disturbed by the machining process, which results in increasing the number of edge atoms. This behaviour is expected for all graphite types and specimens, even if it is only observable at low mass losses.

At 800 K, most specimens exhibit a nearly linear mass loss with increasing heating duration (Fig. 1). From this linear behaviour, the erosion rates are determined (Fig. 2). After 25.5 h, the total mass loss ranges from 2.3 mg for HPG|| to 23 mg for NS31, which is about 3 orders of magnitude higher than at 600 K.

At 900 K, the weight losses are roughly by a factor of 10 higher than at 800 K. In addition to the nearly linear part, a pronounced curvature of the time dependence can be observed in the mass change for AXF-5Q, EK98, and N112, indicating that the erosion rates increase with time, i.e., with burn-off. Such a tendency has also been previously observed for NS31 and N112 [26,28,29] and results from the widening of the pore system, i.e., from increasing the effective surface area. The

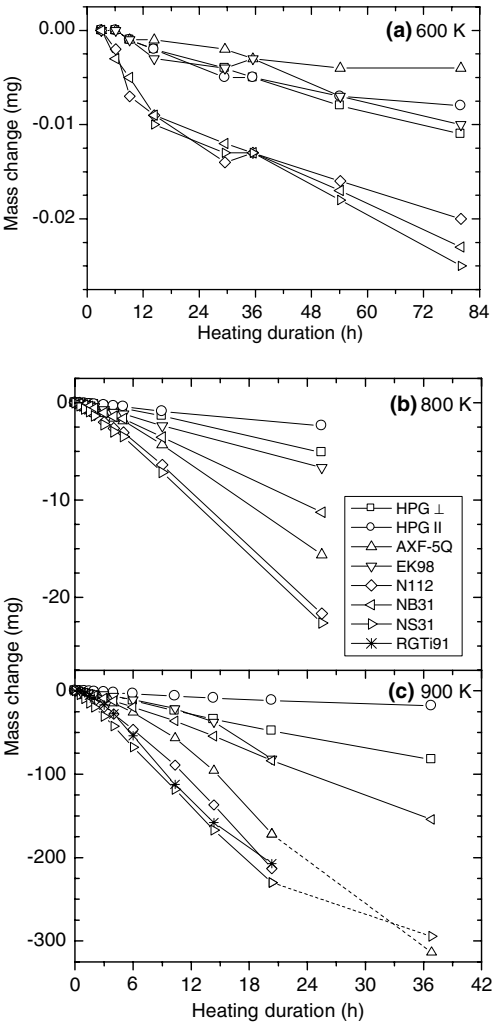

Fig. 1. Mass changes of different types of graphites due to heating in air at 600, 800, and 900 K (a–c) as a function of heating duration. The dashed lines connect data points with low significance after 36.8 h heating.

rates before the increase are plotted in Fig. 2. The rates at higher burn-off, obtained from the data between 14 and 21 h, are in some cases more than twice as high as those at low burn-off (EK98: from 1.6 to 4.9 mg/m^2 s, AXF-5Q: from 4.5 to 9 mg/m^2 s, N112: from 7 to 9 mg/m^2 s).

N112 and NS31 show the strongest erosion at 800 and 900 K. After 20.3 h at 900 K these two materials loose already half of their initial mass, while for HPG|| still 96.8 wt% of the mass remain. After 36.8 h, the N112, EK98, and RGTi91 specimens are either disintegrated to dust or are too fragile to lift them onto the mass balance with a pair of tweezers. The macroscopic surface area of the AXF-5Q specimen is reduced to half of its initial size and to only 8% of its initial mass.

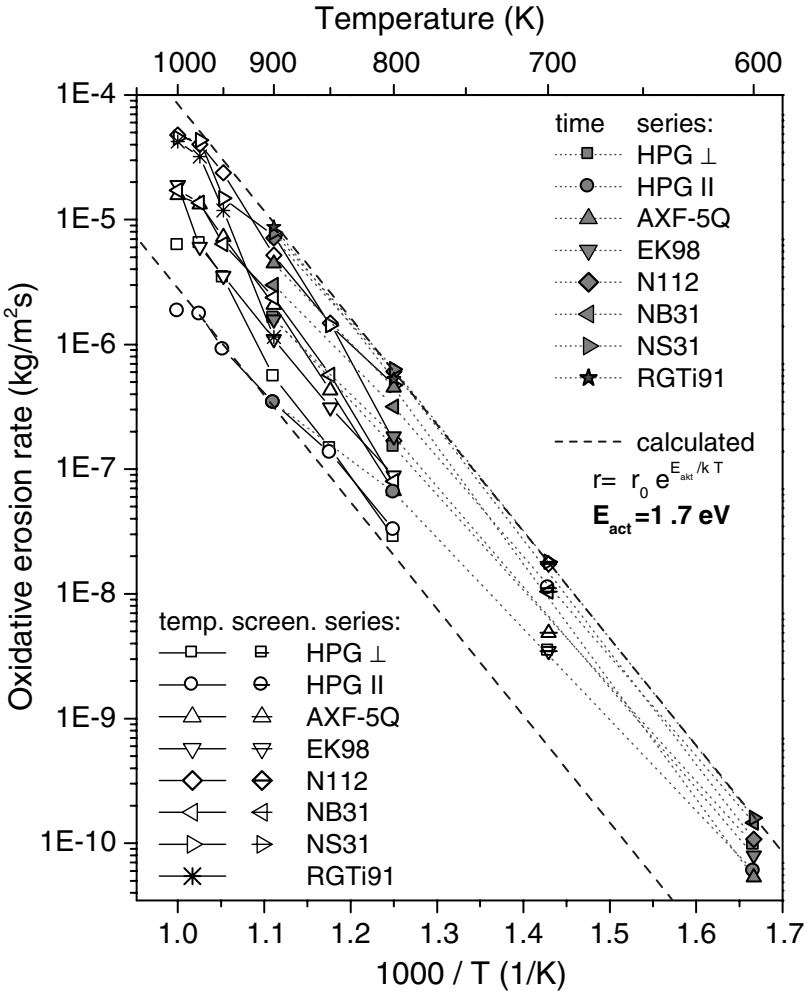

Fig. 2. Oxidative erosion rates versus reciprocal temperature determined from the three 'time series' (600, 800, and 900 K: grey-filled symbols), from the 'temperature series' (800–1000 K: open symbols), and from the 'screening series' (700 K: crossed symbols). For obtaining the erosion rates a surface area of 4 cm^2 is used for all specimens. The dashed lines represent two rates calculated with an activation energy of 1.7 eV differing only in the pre-factor r_0 by a factor of 30.

For the NS31 specimen, 17% of its initial mass is left. After such significant changes, meaningful results are not obtainable and, therefore, the respective points are specially labelled (dashed lines) or not even displayed in Fig. 1.

3.1.2. 'Temperature series' from 600 to 1000 K and erosion rates

Fig. 2 displays the mass losses after heating the specimens at each temperature for 1 h, i.e., the oxidative erosion rates in kg/m^2 s, as a function of the reciprocal temperature. The rates fit to a temperature dependence in accordance with an activation energy of 1.7 eV, which is in agreement with published values for the oxidation reaction of graphite [23,27,33,34,51–54]. But the rates of erosion vary by a factor of up to 30 for the different types of graphite, which can be seen in this plot as a vertical shift of the dashed lines.

For 1 h heating at 600 K the mass changes are below 2 μg, which is the resolution of the used balance. At 800 K for 1 h heating, mass changes up to 700 μg (NS31) are reached, while the lowest loss is just above 40 μg (HPG⊥). At 1000 K the N112 and NS31 specimens loose about one sixth of their initial mass within 1 h. Because of this strong mass loss together with the uncertainties in the temperature due to working with the furnace at its limit, the reliability of the data points at 1000 K is lower, but they still fit quite well in the overall trend (Fig. 2).

The oxidative erosion rates obtained from the three 'time series' (600, 800, and 900 K; Section 3.1.1) and from the mass changes at 700 K of the 'screening series'

are inserted into Fig. 2 to complete the data at lower temperatures. The data points at 800, 900, and 1000 K of the 'screening series' as well as the rates obtained from the mass loss after only 1 h of the 'time series' at 800 and 900 K differ all by less than a factor of two compared to the presented data of the 'temperature series'.

For the series below 750 K, the rates for the different specimens vary only by a factor of five compared to a factor of 30 for temperatures above 750 K (Fig. 2). For these series the rates for the low eroding materials (HPG∥, HPG⊥, AXF-5Q, and EK98) might be overestimated either by measuring very close to the resolution of the balance or by still eroding the surface layer with disturbed graphitic order [49,50].

Overall, the low temperature data (<1000 K) are within the range described by the activation energy of 1.7 eV, and the rates vary by a factor of ≃30 due to differences, e.g., in porosity, grain size, graphitisation degree, i.e., more generally, in the active surface of the materials.

3.2. Oxygen uptake

The oxygen content of the material before and after heating was determined by ion beam analysis. The oxygen content in unheated specimens is below the detection limit of 0.3 at.% for proton scattering (Fig. 3). In the pure graphites after heating for 1 h at 800 and 1000 K, oxygen is found, but only in a thin surface layer of less than 500 nm and always less than 0.7 at.%. The mass gain by this oxygen uptake (<8 μg) is negligible compared to the mass loss under these conditions. In depths larger than 500 nm, the oxygen content is below the detection limit of 0.3 at.%. The surface roughness is not taken into account for this analysis. The creation of stable surface oxygen complexes was observed earlier [49]. In the Si-doped NS31 less than 2 at.% O is found in the surface layer of 500 nm (Fig. 3).

After the erosion experiment, the specimens of the 600 K 'time series' were exposed to air containing water vapour at room temperature for 75 days. Their mass gain by absorption was between 11 μg (HPG⊥) and 62 μg (NS31). These mass gains are assumed to be mainly caused by absorption of water into the pore system and onto the activated surface. In spite of this, the oxygen content of the specimens after these 75 days was below the detection limit of the ^{4}He scattering of 1 at.% O.

Similar mass changes due to absorption are observed for the specimens at the beginning of the 600 K 'time series'. The erosion measurements of these specimens started more than one year after the degassing in vacuum at ≃1020 K, which led to a mass loss ≃15 μg for HPG and ≃40 μg for the other graphites after the first three hours of heating. The whole mass loss within these first three hours was attributed to desorption of water.

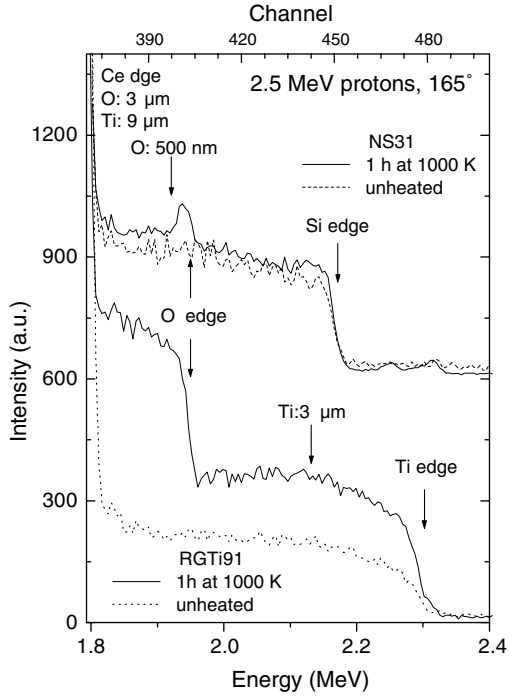

Fig. 3. Spectrum of backscattered protons from NS31 (top) and RGTi91 (bottom) at a scattering angle of 165° and an initial energy of 2.5 MeV. The energy of the backscattered protons is related to a depth scale in which lower energies correspond to larger depths. For each element the zero point of the depth scale is different and is determined by kinematics. It is marked in the figure as Si, C, O, and Ti edge. Additionally, the energy corresponding to a depth of roughly 0.5, 3, and 9 μm for the O and Ti signal is marked. The signals of different elements are added up. The spectra of NS31 are shifted vertically for better visibility.

3.3. Surface morphology of initial and heated specimens

All specimens from the 600, 800, and 900 K 'time series' as well as unheated specimens were analysed by scanning electron microscopy. In Figs. 4–11 the morphology of initial specimen surfaces and specimens which were heated in air for 36.8 h at 900 K are presented.

The specimens heated at 600 K for 80 h do not exhibit visible signs of erosion compared to the unheated specimens. The maximal measured weight loss suggests an average loss in the specimen thickness of less than 0.07 μm over the macroscopic surface area of 4 cm^2. Due to the roughness of the initial surfaces (Figs. 4–11), the absence of visible changes in the initial surface morphology is to be expected.

The specimens heated at 800 K for 25.5 h have mass losses nearly 3 orders of magnitude higher than the 600 K specimens. The averaged thickness losses are between 2.4 μm (HPG∥) and 28 μm (NS31). Despite the

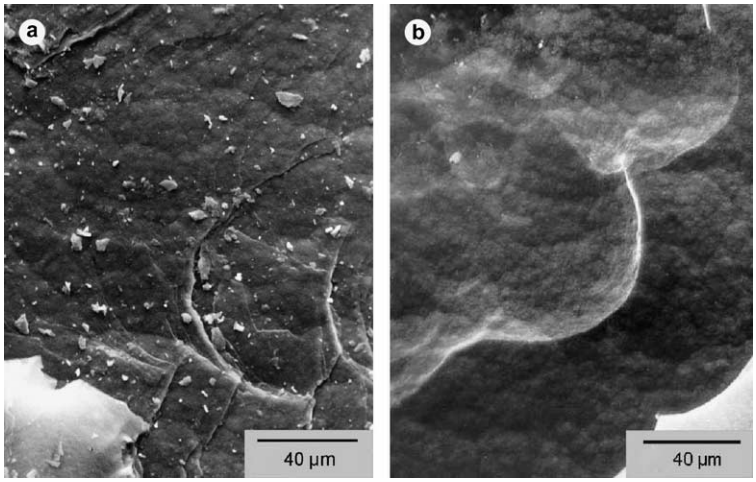

Fig. 4. The regularly terraced surface morphology of HPG‖ (pyrolytic graphite cut parallel to the preferred orientation of the graphitic planes) before (a) and after (b) heating in air for 36.8 h at 900 K.

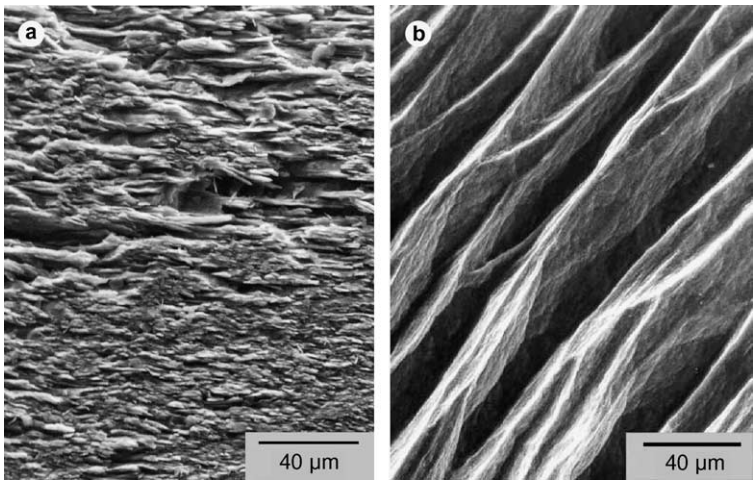

Fig. 5. Structured surface morphology of HPG⊥ (pyrolytic graphite cut perpendicular to the preferred orientation of the graphitic planes) before (a) and after (b) heating in air for 36.8 h at 900 K.

significant losses in thickness, even these specimens show only small changes in the surface morphology compared with the unheated ones. Nevertheless, a tendency to roughen the surface is observed.

The mass loss for the specimens of the 900 K 'time series' (36.8 h) exceeds that of the 800 K 'time series' by more than a factor of 10. These drastic mass losses are accompanied by significant surface morphology changes. The roughness increases strongly. For all specimens, except for the HPG‖. It should be noted that the severe erosion of some of the graphites at 900 K is not evident from the images (Figs. 5–11): The burn-off of the AXF-5Q specimen is more than 90 wt%. For N112, only the fibres remain and the matrix is almost completely eroded, while for NB31 and NS31, the fibres are eroded and a frame of the matrix is left. The NS31 specimen has many voids straight through its 1 mm thickness. The variations in the erosion rates of matrix and fibres are well known and model descriptions have been recently published [51–53,55]. The RGTi91 specimen is pulverised and lost all structural stability.

The following features of the surface morphology before and after heating are observed for the different types of graphite:

• *Pyrolytic graphite:* For the unheated HPG‖ specimens (Fig. 4), small grains of graphite stemming from the cutting procedure are visible on top of the regular pattern of graphite layers. These fragments are eroded partly after heating at 800 K and completely after heating at 900 K. They would be preferentially eroded

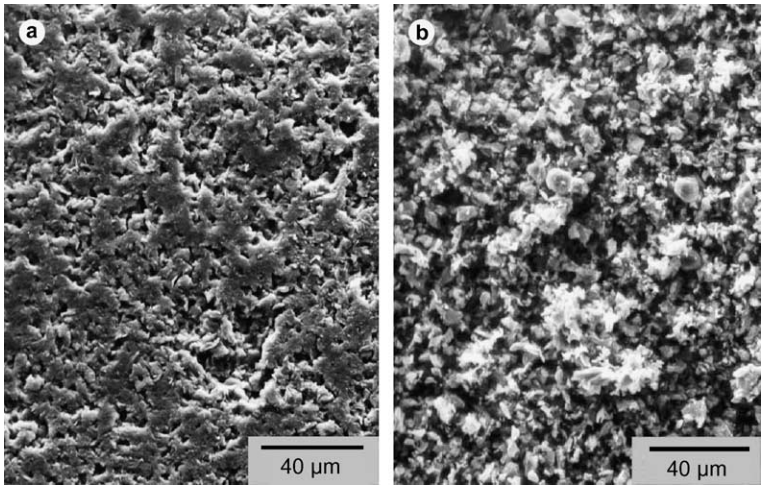

Fig. 6. Random surface morphology of fine-grain graphite AXF-5Q before (a) and after (b) heating in air for 36.8 h at 900 K.

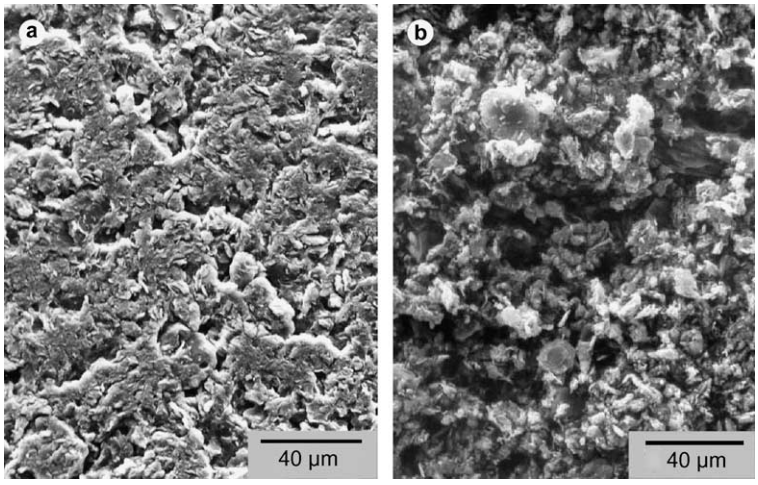

Fig. 7. Random surface morphology of fine-grain graphite EK98 before (a) and after (b) heating in air for 36.8 h at 900 K.

according to previous studies [49,50]. The underlying regular structure, however, is still unchanged, only a few terrace edges show erosion patterns. For HPG⊥, some graphite planes are eroded into parallel grooves (Fig. 5), which already appear on the 800 K 'time series'. The scratch marks from cutting of specimens are still observable after heating.

• *Fine-grain graphites:* For AXF-5Q (Fig. 6) the scratch marks from cutting the specimens disappear due to heating at 900 K, indicating substantial erosion. For AXF-5Q and EK98 (Figs. 6 and 7) the fine graphite grains are clearly visible, but the difference in erosion is not apparent from the images. The erosion of AXF-5Q with open pores is about twice as much as the erosion of EK98 with closed pores. The surface morphology of the AXF-5Q and EK98 specimens from the 800 K 'time series' is barely rougher than the morphology of the unheated ones.

• *Carbon fibre reinforced composite materials* (*CFC*)*:* The unheated specimen of N112 (Fig. 8) shows an ordered 3-dimensional grid of carbon fibres. After heating at 800 K, a gap between fibre and matrix is formed, and after 900 K, erosion of the specimen is clearly visible. Merely a loose grid of carbon fibres remains in the original dense structure. The fibres are more resistant against erosion due to heating in air than the matrix material, which disappears almost completely [51,55].

For the NS31 specimen (Fig. 10) only a frame of hollow tubes remains after heating at 900 K. EDX analysis reveals that this frame consists of Si and C with a ratio

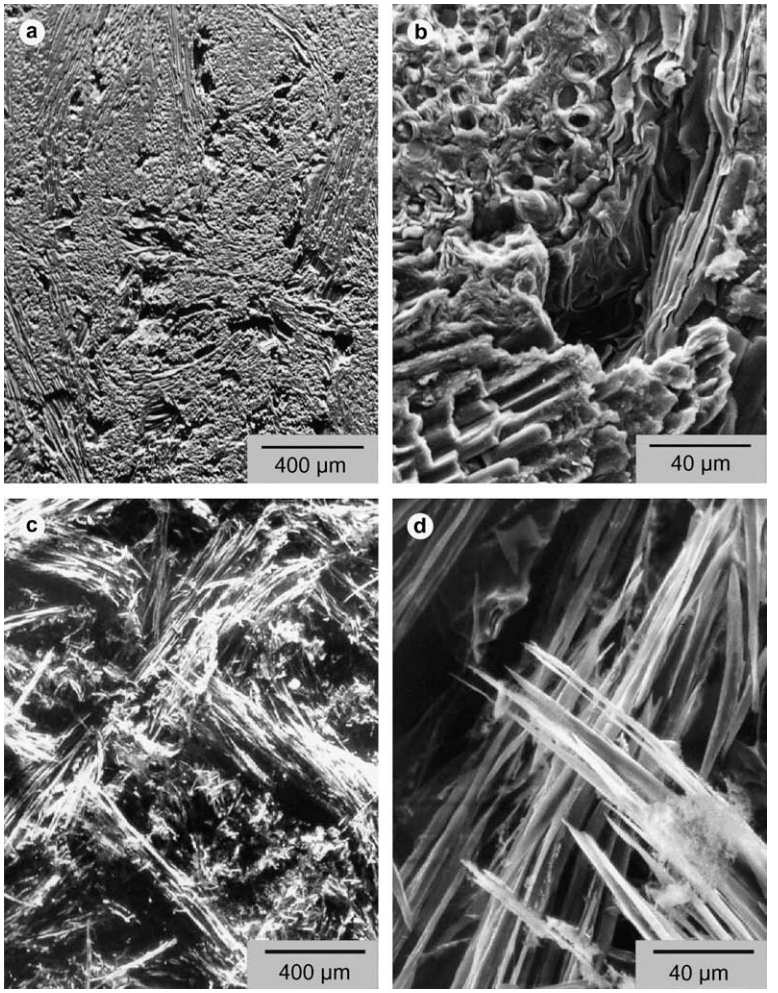

Fig. 8. Surface morphology of the carbon fibre composite N112 before (a, b) and after (c, d) heating in air for 36.8 h at 900 K in two magnifications. In the low magnification images, the fibre bundles with different orientation are visible, while the higher magnified images show the individual fibres surrounded by the matrix (b) and the fibres alone (d).

of roughly 1. Only traces of O are detected as an impurity. The heated NB31 specimen (Fig. 9) with significantly lower erosion still contains more matrix material. The carbon fibres of NB31 seem to be eroded from the outside; only thin fibres of the original carbon fibre structure and of the surrounding matrix material still survive (in contrast to N112). The erosion starts with opening a gap between fibre and matrix as it is observed after 800 K 'time series' for NB31, NS31, and N112. Also after heating for 1 h at 1000 K, the NB31 and NS31 specimens develop such gaps. Additionally, the fibre cross-sections are sometimes smooth, but more often they are deeply grooved (Fig. 12), also after the 800 K 'time series'. In the NS31 specimen after heating at 900 K, however, carbon in the fibres is eroded completely, leaving only a shell of Si or SiC. Such a shell has been observed already on unheated material [41]. The bright areas on the unheated surface (Fig. 10(a)) correspond to high Si contents.

From the description above, it can be concluded that the effective surface area, which is active to the oxidative erosion, is differently increased depending on the inner structure consisting of grains, their orientation, pores, matrix, and fibres. The difference in the erosion behaviour causes the variety of the strongly roughened surface morphology with its appearance on different length scales.

3.4. Ti-doped RGTi91

While all the other investigated graphites present similar oxidative erosion behaviour, RGT91 specimens show a considerable deviation. Therefore, they are studied in more detail.

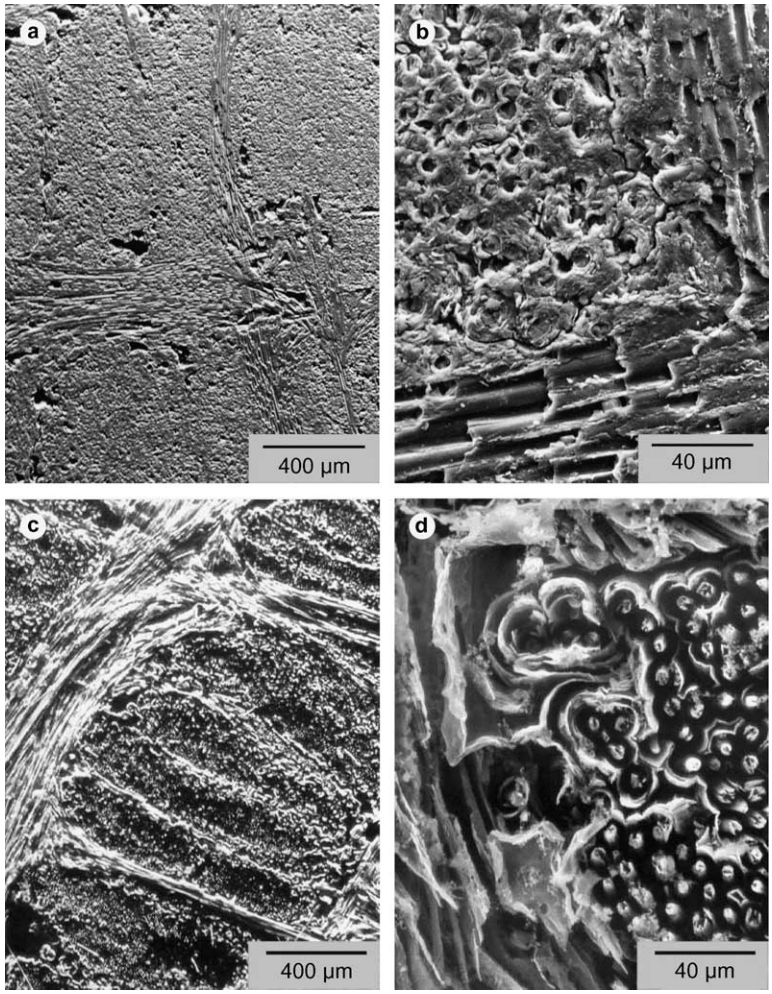

Fig. 9. Surface morphology of carbon fibre composite NB31 before (a, b) and after (c, d) heating in air for 36.8 h at 900 K in two magnifications. The 3-dimensional fibre architecture is visible, resolving single fibres in cross-section and longitudinal section. After heating, gaps exist between the thinned fibres and their surrounding matrix (d).

In Fig. 13, the mass changes of the specimens for the three 'time series' are plotted as a function of the heating duration. At 600 K, the mass of the specimen increases steadily, first weakly (<15 h) then strongly (>30 h). In the first fifteen hours, the specimen gains about 0.15 mg, corresponding to 0.04 wt%. The relative weight change is indicative for a volume process (see below). After 80 h the mass increases by about 57 mg (1.4 wt%), It can be assumed that the change in mass corresponds entirely to an uptake of oxygen and that the superimposed carbon erosion at this temperature is negligible (compare Fig. 1).

After 5 h at 800 K (Fig. 13), the mass of the RGTi91 specimen increases by 2.1 mg (0.5 wt%), while the other investigated graphite specimens loose between 0.4 mg and 3.5 mg (0.1 wt% and 1 wt%). Further heating decreases the weight and for even longer heating durations an erosion of the specimen with rates similar to those of the strongly eroding graphites (N112, NS31, AXF-5Q) of about 0.6 mg/m^2 s occurs.

The results suggest that at 800 K a saturation of the oxygen uptake appears. This behaviour is superimposed with a simultaneously ongoing erosion process, which is stronger at 800 K than at 600 K and becomes evident through the decrease in mass once the oxygen is saturated.

At 900 K erosion dominates and an increase in mass due to oxygen absorption is not observed at all. The oxygen uptake is merely recognised by a change in curvature of the graph in Fig. 13 at low heating durations. Extrapolating the almost linear section at longer durations ($\simeq$9 mg/m^2 s; see Fig. 1(d)) to zero indicates that

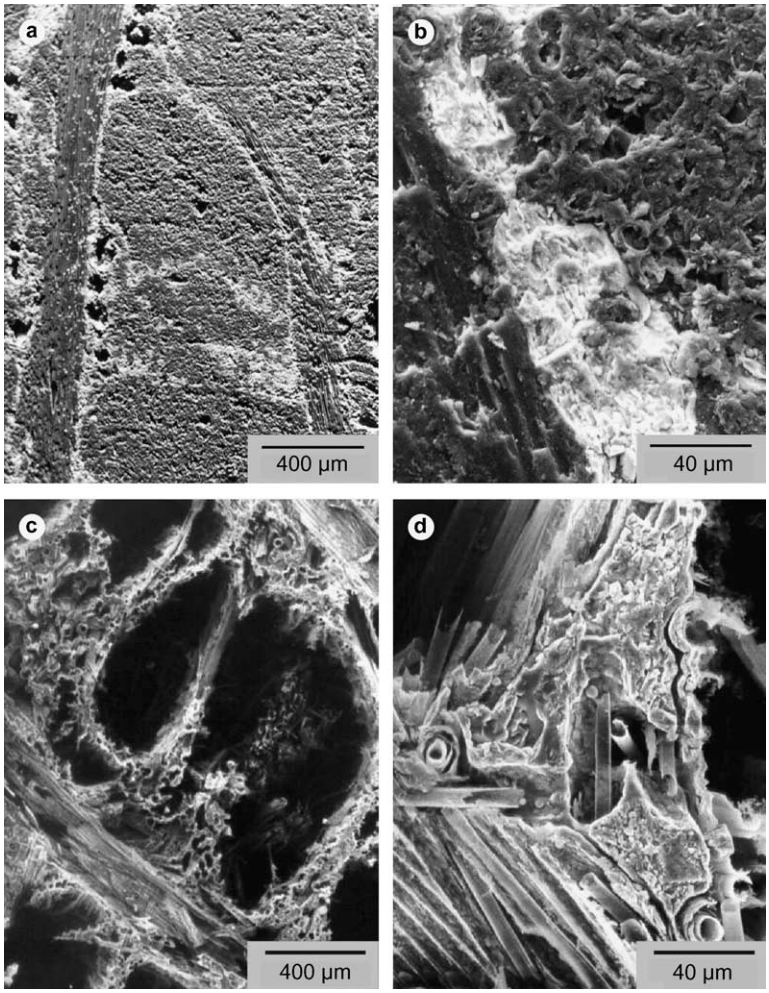

Fig. 10. Surface morphology of carbon fibre composite NS31 before (a, b) and after (c, d) heating in air for 36.8 h at 900 K in two magnifications. The Si or rather SiC is visible as bright areas (a, b). After heating, the 3-dimensional fibre architecture is even clearer visible than that of NB31 (Fig. 9). The core of fibres is completely eroded and only frames of the fibres remain (d).

approximately 25 mg oxygen is taken up (dashed line in Fig. 13), which corresponds to an increase of approximately 6.5 wt%.

On the surface of the unheated RGTi91 specimen, domains of Ti are visible as bright spots in the micrographs (Fig. 11(a)). Heating at 900 K for 36.8 h turns the specimen into powder (Fig. 11(b)). Perhaps the material cracks due to the volume increase by oxidation of the titanium. EDX analysis shows that this powder contains substantial quantities of Ti, O, C, and Si. Low amounts of Si were already observed on initial RGTi91.

The chemical reaction of oxygen with Ti appears to be a reasonable explanation. Analysis by proton scattering indicates no significant uptake of oxygen in the other graphites beyond a thin surface layer (see Section 3.2, Fig. 3). The composition of the RGTi91 specimen after 36 h at 900 K could not be determined with ion beam analysis because the material disintegrated. But for the specimen heated at 700, 800, and 1000 K an oxygen content is found throughout the analysed depth of several microns, e.g., for 1 h at 1000 K, titanium is enriched from about 2 at.% to 4 at.% and the oxygen content from 0 to about 7 at.% (Fig. 3). It has to be noted that the enrichment of Ti is expected due to the carbon burn-off. The observed oxygen content implies that the Ti in the specimen is oxidised. Whether stoichiometric TiO_2 or other titanium oxides are created, could not be distinguished from these measurements. Assuming an uptake of two O atoms per Ti atom, the 2 at.%. Ti-doped specimen should increase by 5 wt%. Oxygen uptake in a graphite specimen containing Ti has also been observed previously [28,35].

The ion beam analysis further showed that the Ti edge of the unheated RGTi91 is rounded (Fig. 3),

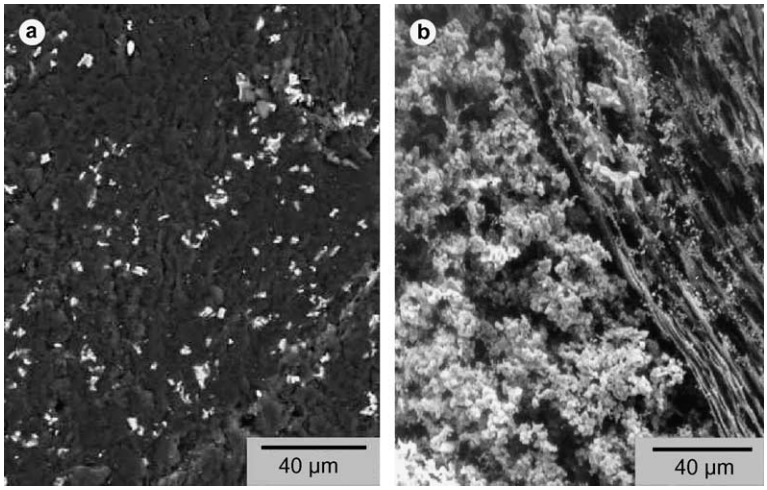

Fig. 11. Surface morphology of Ti-doped graphite RGTi91 before (a) and after (b) heating in air for 36.8 h at 900 K. The bright spots in (a) originate from TiC grains, while the eroded surface is very rough and porous, which overrides the material contrast between TiC and C (b).

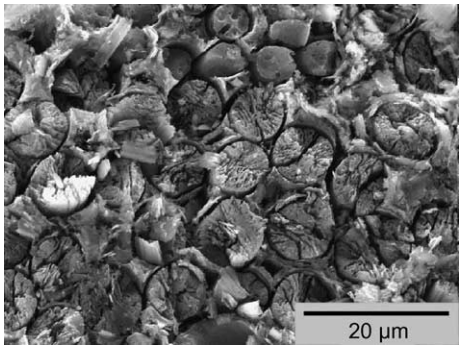

Fig. 12. Surface morphology of fibre cross-sections of the carbon fibre composite NS31 after heating in air for 25.5 h at 800 K, The gap between fibres and matrix as well as the roughened fibre cross-sections are the dominating erosion features of areas with fibres perpendicular to the surface.

indicating depletion of Ti near the surface. The initial deficit of Ti on the surface of the RGTi91 specimen results from the machining: the cutting process dislodges grains of hard TiC that are embedded in the softer graphite from the surface layer of the specimen [56], thus reducing the Ti fraction therein up to the depth of the carbide grain size (≃3 μm, Fig. 3).

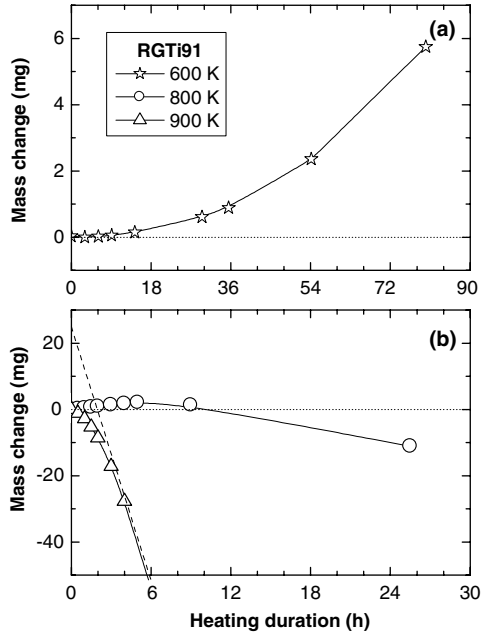

Fig. 13. Mass changes of RGTi91 due to heating in air at 600 (a), 800, and 900 K (b) as a function of heating duration. The dashed line is an extrapolation of the data at longer heating durations at 900 K to zero duration (Fig. 1).

4. Summary

The oxidative erosion of seven types of graphite was investigated by heating in air at temperatures between 600 and 1000 K. The temperature dependence of the oxidative erosion rate was determined from several series of heating experiments. The HPG‖ type is the most stable material against oxidative erosion, with erosion rates of about 0.07 mg/m^2 s at 800 K and 0.34 mg/m^2 s at 900 K, while the rate for the other graphite types are up to a factor of 30 higher.

The observed curvature in the mass change with heating duration for some types of graphite (EK98, AXF-

5Q, and N112) indicates an increasing rate at higher burn-off (Fig. 1). This cannot be explained by an uptake of oxygen as for the RGTi91 specimens. An increasing erosion rate points to an enhancement of the total exposed surface area of the specimens. This could be due to the fact that new pores in the bulk of the graphite are opened as the surface of the specimen is eroded, giving way to a higher erosion rate and intensifying the exchange of gases. Remember that the experimental conditions belong to the regime limited by in-pore diffusion or even by the chemical reaction between oxygen and carbon [26–28]. With respect to this understanding, the slopes occurring in Fig. 2 should represent the activation energy of the chemical process. All data are well described by an activation energy of 1.7 eV, in good agreement with the literature [23,27,33,34,51–54].

For further analyses and models, it is necessary to determine the actual active surface area of the specimens and its evolution with burn-off. So far, only the visible geometric surface of approximately 4 cm^2 is known. Erosion, however, presumably depends on the effective surface area, which is correlated with the porosity. It is conceivable that this does not only vary significantly between different graphites, but also between two specimens of the same graphite. A change of the effective surface area during a sequence of measurements is also conceivable. The variety of drastic changes of the surface morphology observed with SEM indicates that the effective surface area is increased by a different erosion behaviour of grains, pores, matrix, and fibres.

The high erosion rates of NS31 above 800 K, which are about twice that of the similar NB31 without Si, indicate that either the microstructure of the two materials differs or that Si might act as a catalyst, supporting the oxidative erosion of the graphite rather than preventing it. The second explanation is supported by recent results of Anderl et al. [26]. The temperatures reached in the present study are too low for the formation of a protective SiO_2 layer, as reported for 1273 K [30,36].

Ion beam analysis confirms that the Ti-doped RGTi91 specimen incorporates significant amounts of oxygen – around 5% of its initial mass. The other graphites, in particular the Si-doped NS31, do not exhibit this behaviour.

5. Conclusion

As a final conclusion, the removal of co-deposited amorphous hydrocarbon layers in fusion devices by oxidation in an oxygen atmosphere at $\simeq$650 K will not lead to significant erosion of the carbon base material. The erosion rates of deposited layers from fusion devices exceed the rates of amorphous hydrocarbon layers obtained in laboratory coating devices ($\simeq$0.03 mg/m^2 s; $\simeq$0.06 μm/h [10]) by 1 to 3 orders of magnitude (>10 μm/h) [8,10,12,14]. The removal rates of these laboratory layers at 650 K are, however, already one order of magnitude higher than those of the carbon base materials. But for future applications of carbon in fusion plasma environments, also irradiation effects have to be considered.

Acknowledgments

The authors would like to thank W. Ottenberger for preparing the specimens and Dr H. Maier for fruitful discussion during preparation of the paper.

References

[1] G. Federici, R.A. Anderl, P. Andrew, J.N. Brooks, R.A. Causey, J.P. Coad, D. Cowgill, R.P. Doerner, A.A. Haasz, G. Janeschitz, W. Jacob, G.R. Longhurst, R. Nygren, A. Peacock, M.A. Pick, V. Philipps, J. Roth, C.H. Skinner, W.P. Wampler, J. Nucl. Mater. 266–269 (1999) 14.
[2] G. Janeschitz, ITER JCT, and HTs, J. Nucl. Mater. 290–293 (2001) 1.
[3] G. Federici, J.N. Brooks, D.P. Coster, G. Janeschitz, A. Kukuskhin, A. Loarte, H.D. Pacher, J. Stober, C.H. Wu, J. Nucl. Mater. 290–293 (2001) 260.
[4] E. Vietzke, A.A. Haasz, in: W.O. Hofer, J. Roth (Eds.), Physical Processes in Plasma–wall Interaction in Nuclear Fusion, Academic Press, New York, 1996, p. 135.
[5] J. Roth, J. Nucl. Mater. 266–269 (1999) 51.
[6] International Atomic Energy Agency, ITER EDA Documentation Series, No. 24, IAEA, Vienna, 2002.
[7] R.A. Causey, W.L. Chrisman, W.L. Hsu, R. Anderl, B. Wishard, J. Vac. Sci. Technol. A7 (1989) 1078.
[8] R.A. Causey, W.R. Wampler, D. Walsh, J. Nucl. Mater. 176&177 (1990) 987.
[9] A.A. Haasz, S. Chiu, J.E. Pierre, Y.I. Gudimenko, J. Vac. Sci. Technol. A14 (1996) 184.
[10] W. Wang, W. Jacob, J. Roth, J. Nucl. Mater. 245 (1997) 66.
[11] S. Alberici, J.P. Coad, H.-K. Hinssen, R. Moormann, P. Wienhold, C.H. Wu, J. Nucl. Mater. 258–263 (1998) 764.
[12] K. Maruyama, W. Jacob, J. Roth, J. Nucl. Mater. 264 (1999) 56.
[13] V. Philipps, H.G. Esser, J. von Seggern, H. Reimer, M. Freisinger, E. Vietzke, P. Weinhold, J. Nucl. Mater. 266–269 (1999) 386.
[14] J.W. Davis, A.A. Haasz, J. Nucl. Mater. 266–269 (1999) 478.
[15] S. Alberici, H.-K. Hinssen, R. Moormann, C.H. Wu, J. Nucl. Mater. 266–269 (1999) 754.
[16] M. Balden, M. Mayer, J. Nucl. Mater. 283–287 (2000) 1057.
[17] M. Balden, M. Mayer, J. Nucl. Mater. 298 (2001) 225.
[18] K. Maruyama, W. Jacob, J. Roth, Jpn. J. Appl. Phys. 40 (2001) 788.
[19] A.V. Markin, A.E. Gorodetsky, A.P. Zakharov, J. Nucl. Mater. 248 (1997) 34.

[20] R.D. Penzhorn, N. Bekris, W. Hellriegel, H.-E. Noppel, W. Nägele, H. Ziegler, R. Rolli, H. Werle, A. Haigh, A. Peacock, J. Nucl. Mater. 279 (2000) 139.
[21] J.W. Davis, C.G. Hamilton, A.A. Haasz, J. Nucl. Mater. 288 (2001) 148.
[22] G. Klages, M. Balden, W. Jacob, J. Roth, in: 9th International Workshop on Carbon Materials, Hohenkammer, Germany, 2000, unpublished data.
[23] J.W. Davis, A.A. Haasz, Phys. Scr. T 91 (2001) 33.
[24] J. Raeder, S. Piet, R. Buende, E. Ebert, W. Gulden, H. Iida, B. Kolbasov, N. Mitchell, Y. Seki, L. Topilski, H. Yoshida, ITER Documentation Series, No. 36, IAEA, Wien, 1991.
[25] B.J. Merrill, M.H. O'Brien, in: IEEE 13th Symposium on Fusion Engineering, vol. 2, 1990, p. 1487.
[26] R.A. Anderl, R.J. Pawelko, G.R. Smolik, G. Piazza, F. Scaffidi-Argentina, L.L. Snead, J. Nucl. Mater. 307–311 (2002) 1375.
[27] P.L. Walker, F. Rusinko, L.G. Austin, Advances in Catalysis, vol. XI, Academic Press, New York and London, 1959.
[28] R. Moormann, H.-K. Hinssen, A.-K. Krussenberg, B. Stauch, C.H. Wu, J. Nucl. Mater. 212–215 (1994) 1178.
[29] A.-K. Krüssenberg, R. Moormann, H.-K. Hinssen, M. Hofmann, C.H. Wu, J. Nucl. Mater. 258–263 (1998) 770.
[30] C.H. Wu, C. Alessandrini, P. Bonal, H. Grote, R. Moormann, M. Rödig, J. Roth, H. Werle, G. Vieider, J. Nucl. Mater. 258–263 (1998) 833.
[31] D.R. Olander, W. Siekhaus, R. Jones, J.A. Schwarz, J. Chem. Phys. 57 (1972) 408.
[32] D.R. Olander, R.H. Jones, J.A. Schwarz, W.J. Siekhaus, J. Chem. Phys. 57 (1972) 421.
[33] F.M. Lang, P. Magnier, in: P.L. Walker (Ed.), Chemistry and Physics of Carbon, vol. 3, Marcel Dekker, New York, 1968, p. 121.
[34] M.F.R. Mulcahy, First BOC Priestley Conference, Leeds, The Chemical Society, London, 1978, p. 175.
[35] A.Y.K. Chen, A.A. Haasz, J.W. Davis, J. Nucl. Mater. 227 (1995) 66.
[36] C.H. Wu, C. Allesandrini, R. Moormann, M. Rubel, B.M.U. Scherzer, J. Nucl. Mater. 220–222 (1995) 860.
[37] M. Balden, Phys. Scr. T 81 (1999) 64.
[38] C. García-Rosales, M. Balden, J. Nucl. Mater. 290–293 (2001) 173.
[39] M. Balden, J. Roth, J. Nucl. Mater. 280 (2000) 39.
[40] W. Eckstein et al. (Eds.), Particle Induced Erosion of Be, C and W in Fusion Plasmas, Part B: Physical Sputtering and Radiation-Enhanced Sublimation, Atomic and Plasma-material Interaction Data for Fusion 7, Part B, IAEA, Vienna, 2001.
[41] M. Balden, J. Roth, C.H. Wu, J. Nucl. Mater. 258–263 (1998) 740.
[42] C. García-Rosales, J. Roth, R. Behrisch, J. Nucl. Mater. 212–215 (1994) 1211.
[43] G. Kalinim, V. Barabash, A. Cardella, J. Dietz, K. Ioki, R. Matera, R.T. Santoro, R. Tivey, The ITER Home Teams, J. Nucl. Mater. 283–287 (2000) 10.
[44] V. Barabash, M. Akiba, J.P. Bonal, G. Federici, R. Matera, K. Nakamura, H.D. Pacher, M. Rödig, G. Vieider, C.H. Wu, J. Nucl. Mater. 258–263 (1998) 149.
[45] S. Brunauer, P.M. Emmett, E. Teller, J. Am. Chem. Soc. 60 (1938) 309.
[46] W.-K. Chu, J.W. Mayer, M.-A. Nicolet, Backscattering Spectrometry, Academic Press, New York, 1978.
[47] M. Mayer, SIMNRA User's Guide, Tech. Rep. IPP 9/113, Max-Planck-Institut fur Plasmaphysik, Garching, 1997.
[48] Institute Dr. Klingele, Adelgundenstr. 8, D-80538 München.
[49] F. Rodriguez-Reinoso, P.A. Thrower, P.L. Walker, Carbon 12 (1974) 63.
[50] F. Rodriguez-Reinoso, P.A. Thrower, Carbon 12 (1974) 269.
[51] D.W. McKee, Carbon 25 (1987) 551.
[52] M.-P. Bacos, J.-M. Dorvaux, O. Lavigne, Y. Renollet, Carbon 38 (2000) 77.
[53] M.-P. Bacos, J.-L. Cochon, J.-M. Dorvaux, O. Lavigne, Carbon 38 (2000) 93.
[54] S. Labruquére, H. Blanchard, R. Pailler, R. Naslain, J. Eur. Ceram. Soc. 22 (2002) 1001.
[55] J. Liao, T. Chen, B. Huang, G. Shi, X. Xiong, Carbon 40 (2002) 617.
[56] M. Balden, C. García-Rosales, R. Behrisch, J. Roth, P. Paz, J. Etxeberria, J. Nucl. Mater. 290–293 (2001) 52.